Design of phenanthroline and diindolocarbazole based emitter for efficient upconversion of triplet excitons by improving rISC

Gokul Ganesan[ac,#], *Farah Ansari*[a#], *Vipin Kumar*[d], *Yi-Ting Chen*[e], *Guan-Yu Su*[e], *Prabhakar Chetti*[d], *Chih-Hao Chan*[e,*], *Atul C. Chaskar*[a,b,*]

[a] National Center for Nanosciences and Nanotechnology, University of Mumbai, Vidyanagari, Mumbai 400098, Maharashtra, India

[b] Department of Chemistry, Institute of Chemical Technology (ICT), N.P. Marg, Matunga, Mumbai 400019, India

[c] Department of Chemistry, Jai Hind College, Mumbai 400020, Maharashtra, India

[d] Department of Chemistry, National Institute of Technology, Kurukshetra-136119, India

[e] Department of Electrical Engineering, Yuan Ze University, Taoyuan 32003, Taiwan

* Corresponding authors, Email address: achaskar25@gmail.com (Dr. Atul Chaskar); chc@saturn.yzu.edu.tw (Dr. Chih-Hao Chang)

[#]Authors with equal contribution

Keywords: Diindolocarbazole, Phenanthroline, TADF, OLED, RISC.

Abstract:

There has been significant advancement in display technology in recent times. However, synthetic efforts toward designing more efficient emitters are still underway. TADF emitters offer the advantage of an all organic based design with IQE_{max} of 100%. To study the effect of phenanthroline-based moieties, we designed and synthesized two yellow-green thermally

activated delayed fluorescent (TADF) emitters, **DICz-DBPZ** and **DICz-DPPN**. Due to structural variations associated with steric strain, the two emitters displayed different photophysical and organic light-emitting diode (OLED) performances. For **DICz-DPPN**, the absorption and emission maxima were recorded at 313-368 nm and 516 nm, respectively, while for **DICz-DBPZ**, they were observed at 311-393 nm and 559 nm. The DPPN-substituted TADF emitter had an EQE of 5.0% and color coordinates of (0.37, 0.53), whereas the DBPZ-substituted emitter displayed a high EQE of 15% with color coordinates of (0.47, 0.51). Due to the closed structure of **DICz-DBPZ**, thermal decomposition temperature occurred at 269ºC as compared to 213ºC for **DICz-DPPN**, which significantly influenced the difference in EQE between the two emitters. In order to simultaneously obtain high EQE and a long lifetime, this study offers an approach to synthesize yellow TADF emitters by utilizing a combination of diindolocarbazole (DICz) and 1,10-phenanthroline-5,6-diamine as a stable donor-acceptor.

Introduction:

Following the groundbreaking work by Van Slyke and Tang et al. in 1987, organic light-emitting diodes (OLEDs) are used as economically viable replacements for traditional display and lighting technologies.[1] OLEDs, a subclass of organic-based devices, have revolutionized the display and lighting industries due to their exceptional benefits such as high luminance efficiency, full color/large area displays, wide viewing angles, lightness and transparency, low power consumption, and so on.[2-5]Although the phosphorescent emitters used in modern commercialized OLEDs have 100% efficiency, they have disadvantages such as the use of expensive noble metals, being less ecologically friendly, and having short device lifetimes. Recently, it has also been shown that organic emitters made without metals and using thermally activated delayed fluorescence (TADF) are capable of 100% exciton harvesting.[6], [7] Therefore, for everyday applications, the TADF system combines the desired advantages of cheap cost, energy savings, environmental friendliness, and sustainability.

The majority of TADF emitters are donor (D)-acceptor (A) systems, which have a significant intramolecular charge transfer (ICT) effect that can reduce the singlet-triplet splitting energy (ΔEST) and allow triplet-to-singlet up-conversion via reverse intersystem crossing (RISC). A small ΔEST can be attained by decreasing the overlap between the highest occupied molecular orbital (HOMO) and the lowest unoccupied molecular orbital (LUMO). A high photoluminescence quantum yield (PLQY), which can be achieved by maintaining a maximum

overlap between the HOMO and LUMO in the molecular design, is another need for high-performance TADF emitters.[8] In order to prevent non-radiative loss processes and create pure-colour extremely effective TADF emitter-based OLEDs, molecular designs with controlled donor/acceptor rotation are preferred over those with unrestricted rotation. Therefore, to obtain a high external quantum efficiency (EQE), it is necessary to achieve a balance between a small ΔEST and a high PLQY inside a single organic molecule. [9-14]

In all three colours, the TADF OLEDs' external quantum efficiency (EQE) is close to or above 30%, but their lifetime is substantially shorter than that of fluorescent and phosphorescent OLEDs. [15], [16] The Adachi group presented a device design that would use the TADF material as a sensitizer or assistant dopant for the red, yellow, green, and blue-fluorescent emitters in order to address the short lifetime of the TADF OLEDs.[17]

Because of its strong thermal properties [18], [19], rigid planar structure [20]–[24], and simplicity of structural alteration, phenanthroline demonstrated the proper characteristics as an acceptor. Diindolocarbazole (DICz), which is composed of carbazole units, was selected as a suitable TADF donor after it was shown to reduce the singlet-triplet energy gap (ΔEST) at high reverse intersystem crossing (RISC) rates.[25]

Two novel yellow TADF materials were synthesized consisting of diindolocarbazole as donor and pyrimidine-5-carbonitrile as an acceptor unit. PyCNTruX demonstrated an external quantum efficiency of 21.6%, compared to TCNTruX's 12.8%.[26] Shantaram Kothavale, Won Jae Chung, and Jun Yeob Lee created two isomeric dipyrido[3,2-a:20,30-c]phenazine (DPPZ) acceptors by attaching two 9,9-dimethyl-9,10-dihydroacridine (DMAC) donor units to the ortho (11, 12) and para (10, 13) positions of the DPPZ acceptor. The red TADF-OLED displayed a much greater EQE of 13.4% as compared to the pDMAC-DPPZ-doped OLED, which displayed an EQE of 4.0%.[8]

In this study, we report a diindolocarbazole (DICz) donor and 1,10-phenanthroline-5,6-diamine acceptor derived donor–acceptor combination for the design of two green-yellow TADF emitters, namely 5,10-diphenyl-15-(4-(3-phenylpyrazino[2,3-f][1,10]phenanthrolin-2-yl)phenyl)-10,15-dihydro-5H-diindolo[3,2-a:3',2'-c]carbazole [**DICz-DPPN**] and 12-(10,15-diphenyl-10,15-dihydro-5H-diindolo[3,2-a:3',2'-c]carbazol-5-yl)dibenzo[a,c]dipyrido[3,2-h:2',3'-j]phenazine [**DICz-DBPZ**].

Experimental section

Synthesis

The synthesis of emitters was accomplished using the following synthetic scheme as described.

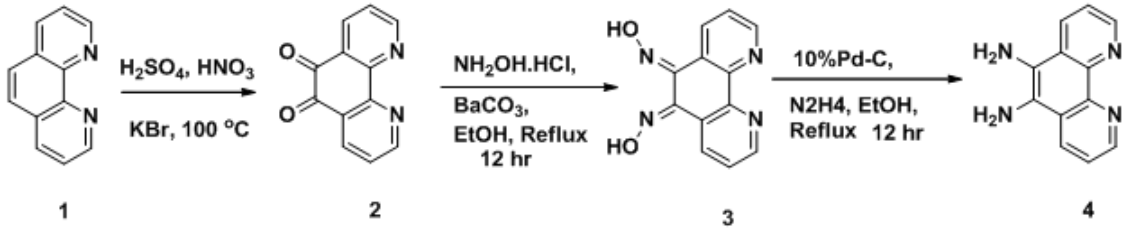

Scheme 1: Synthesis of intermediates (**4**)

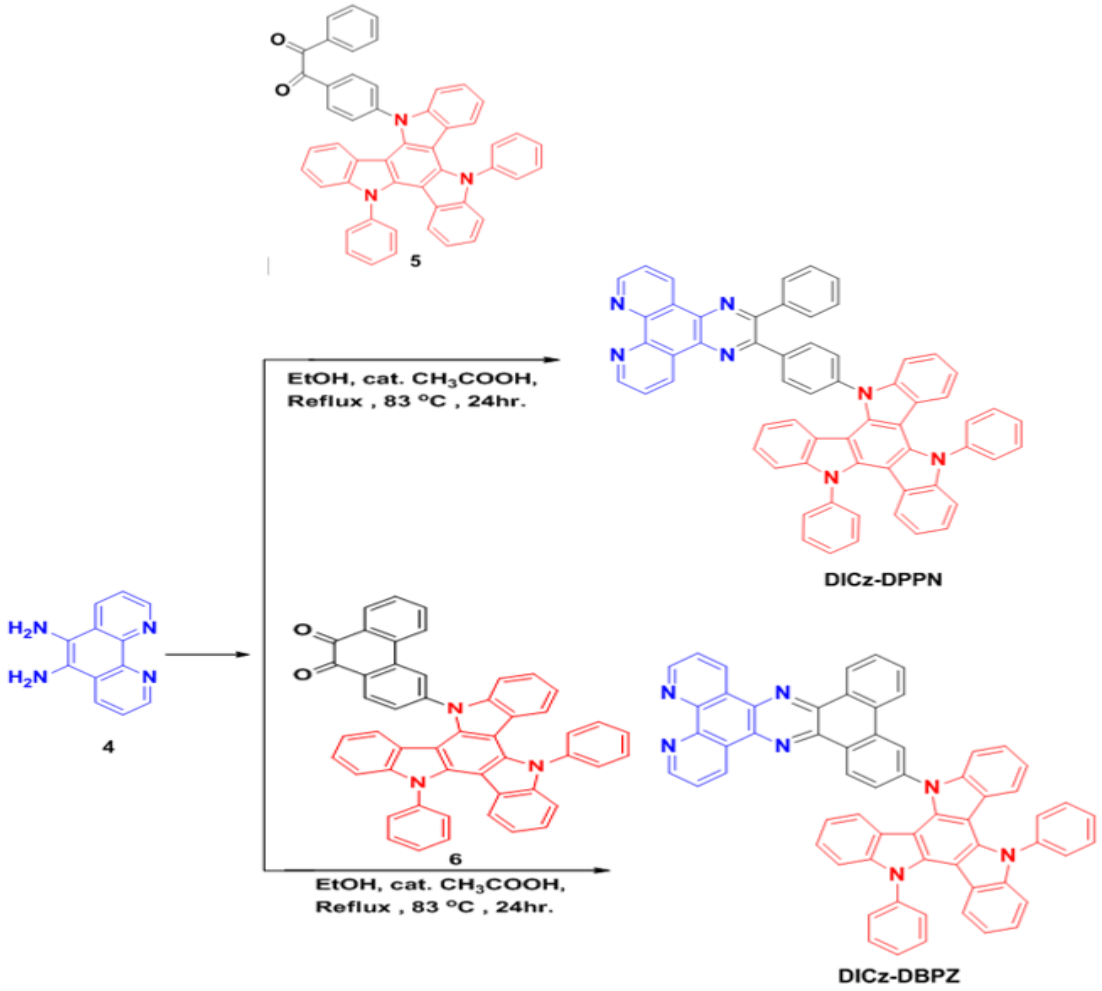

Scheme 2: Synthesis of **DICz-DPPN**, **DICz-DBPZ** from intermediate **4**

The synthesis of the two TADF-based OLED molecules- **DICz-DPPN** and **DICz-DBPZ** is described in **Scheme 1&2** along with their chemical structure. The common intermediate 1,10-phenanthroline-5,6-diamine **[4]** was synthesized by reduction of 1,10-phenanthroline-5,6-dione

dioxime **[3]** and was coupled with 1-(4-(10,15-diphenyl-10,15-dihydro-5H-diindolo[3,2-a:3',2'-c]carbazol-5-yl)phenyl)-2-phenylethane-1,2-dione **[5]** and 3-(10,15-diphenyl-10,15-dihydro-5H-diindolo[3,2-a:3',2'-c]carbazol-5-yl)phenanthrene-9,10-dione **[6]** in ethanol and catalytic amount of acetic acid to give **[DICz-DPPN]** and **[DICz-DBPZ]** in 50% and 55% yields, respectively.

1. Synthesis of 1,10-phenanthroline-5,6-dione [2]

A mixture of 1,1'-phenanthroline (1.0 g) and NaBr (5.7 g, 55 mmol) was added slowly in a flask containing sulphuric acid [20ml], HNO_3 [10ml] was introduced in this solution. This procedure was carried out in an ice bath for 10 minutes. The oil-Water separator was connected to the flask and the mixture was heated to 90^0C for 2 hours. The cooled mixture was poured into ice and $NaHCO_3$ was added to neutralize till pH 6-7 was obtained. The suspension was extracted in CH_2Cl_2 and the organic layer was recrystallized by 95% ethanol.

2. Synthesis of (5E,6E)-1,10-phenanthroline-5,6-dione dioxime [3]

A mixture of 0.420g (2.00 mmol) 1.10-phenanthroline-5 ,6-dione, 0.486g (7.00 mmol) of NH2OH·HCl, and 0.592g of (3.00 mmol) of BaCO3 was refluxed in 30ml of ethanol for 12 hours by constant stirring. The solvent was evaporated by Rotary evaporation and the residue was treated by 40ml of 0.2 M HCL. The mixture was stirred for 30 min and then filtered followed by washing with solvents like water, ethanol and ether. The residue was dried under vaccum at 80^0C to obtain 1,10-phenanthroline-5,6-dione dioxime.

3. Synthesis of 1,10-phenanthroline-5,6-diamine [4]

A mixture of 0.400g (1.63 mmol) of phendioxime and 0.40g of Pd-C (10%) in 100 ml of dry ethanol were purged with N_2 and refluxed at 83^0 C. A solution of 3.50 ml of N2H4.H2O and 15 ml of ethanol was added over a period of an hour while refluxing for 12 hours. The mixture was filtered hot on a bed of celite and was washed with 20 ml of boiling ethanol. The filtrate was dried and triturated with 30 ml of water and left at 4^0 C overnight. The solid was filtered and washed with cold water and dried.

4. Synthesis of 5,10-diphenyl-15-(4-(3-phenylpyrazino[2,3-f][1,10]phenanthrolin-2-yl)phenyl)-10,15-dihydro-5H-diindolo[3,2-a:3',2'-c]carbazole [DICz-DPPN]

Intermediate [5] 1-(4-(10,15-diphenyl-10,15-dihydro-5H-diindolo[3,2-a:3',2'-c]carbazol-5-yl)phenyl)-2-phenylethane-1,2-dione (300mg, 1.023 mmol) and 1,10-phenanthroline-5,6-

diamine [4] (89.31 mg, 1.023 mmol) were dissolved in anhydrous ethanol (10 mL). A catalytic amount of acetic acid was added and the resulting mixture was refluxed for 12 hrs. After cooling to room temperature, the solid precipitated out in the reaction mixture was filtered, washed with DCM, and dried well. The crude product obtained was further purified by column chromatography (3% MeOH in DCM) to obtain the desired product as a yellow solid [55%].

5. Synthesis of 12-(10,15-diphenyl-10,15-dihydro-5H-diindolo[3,2-a:3',2'-c]carbazol-5-yl)dibenzo[a,c]dipyrido[3,2-h:2',3'-j]phenazine [DICz-DBPZ]

Intermediate [6] 3-(10,15-diphenyl-10,15-dihydro-5H-diindolo[3,2-a:3',2'-c]carbazol-5-yl)phenanthrene-9,10-dione (300mg, 1.023 mmol) and 1,10-phenanthroline-5,6-diamine [4] (89.61 mg, 1.023 mmol) were dissolved in anhydrous ethanol (10 mL). A catalytic amount of acetic acid was added and the resulting mixture was refluxed for 12 hrs. After cooling to room temperature, the solid precipitated out in the reaction mixture was filtered, washed with DCM, and dried well. The crude product obtained was further purified by column chromatography (3% MeOH in DCM) to obtain the desired product as Greenish-brown solid [55%].

Photophysical, thermal, electrochemical measurement

All the photophysical measurements in solution were done at a concentration of 10μM in suitable HPLC grade solvents obtained from Sigma-Aldrich. The UV spectra were recorded in Shimadzu Uv-visible Spectrophotometer UV-1780 and the steady state fluorescence spectra were recorded in Shimadzu RF-6000 spectrofluorimeter with an excitation and emission slit bandwidth of 5 nm. TGA was performe using HITACHI STA7300 and a nitrogen environment, at a heating rate of 10^0C/min from up to 600^0C. On a Metrohm Autolab PGSTAT204 Potentiostat/Galvanostat in cyclic voltammetry mode, electrochemical analysis was carried out. As working, counter, and reference electrodes, glassy carbon, Pt wire, and Ag/AgCl, respectively, were used. The electrolytes utilised were tetrabutyl ammonium perchlorate (0.1 mol/L) and tetrabutyl ammonium hexafluorophosphate (0.1 mol/L) at a scan rate of 100 mV/sec.

Fabrication and Characterization of OLEDs

Organic materials purchased from Shine Materials Technology were subjected to temperature-gradient sublimation in a high vacuum before use. After a cleaning procedure of ultrasonication of the ITO-coated glass in deionized water and organic solvents, the ITO substrate was pretreated with plasma for 5 minutes. The organic and metal layers were deposited by thermal evaporation in a vacuum chamber with a base pressure of $< 10^{-6}$ Torr.

Device fabrication was completed in a single cycle without breaking the vacuum. The deposition rate of organic materials was kept at around 0.1 nm s^{-1}. The active area was defined by the shadow mask (2 × 2 mm^2). Current density-voltage-luminance characterization was done using two Keysight B2901A current source-measure units equipped with a calibrated Si-photodiode. The electroluminescent spectra of the devices were recorded using an Ocean Optics spectrometer (Ocean Optics 2000).

Results and Discussion:

Thermal properties:

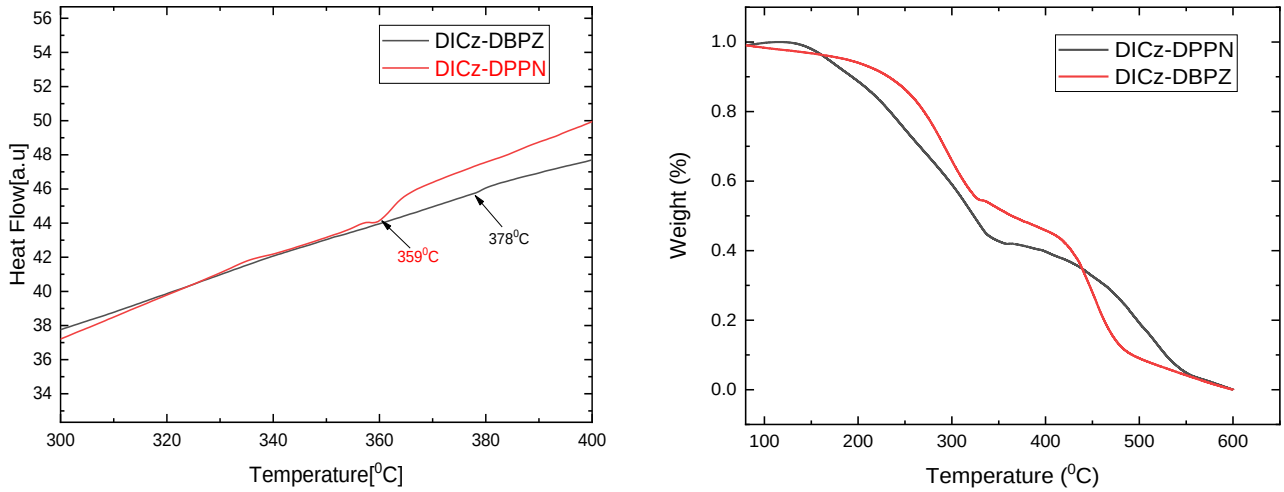

Fig 1: Thermo gravimetric Analysis and Differential scanning calorimetric curves of **DICz-DBPZ** and **DICz-DPPN**.

To determine the glass transition temperature (Tg) and thermal decomposition temperature (Td), **DICz-DPPN** and **DICz-DBPZ** were subjected to thermal analysis using differential scanning calorimetry (DSC) and a thermogravimetric analyzer (TGA) at a heating rate of 10°C min^{-1} under a nitrogen environment. **DICz-DPPN** and **DICz-DBPZ** had measured Tg values of 359°C and 378°C, respectively. Additionally, it was determined that the T_d values of **DICz-DPPN** and **DICz-DBPZ** at 5% weight loss were 213°C and 269°C, respectively which indicates their suitability for vacuum-evaporation-based device fabrication (**Fig. 1**).

Photophysical properties:

Photophysical features of two emitters, including absorption and emission spectra, were examined to determine the influence of two distinct acceptors and a rigid diindolocarbazole (DICz) donor. The high energy absorption peak π-π* was observed from 311-314 nm for the **DICz-DBPZ** molecule, and the n-π* transition was observed from 330-393 nm. The **DICz-DPPN** molecule exhibited absorption from 313-314 nm for the π-π* transition, while the low energy absorption peak n-π* was in the 331-368 nm region. Because the π-π* transition demands a lot of energy, the wavelength decreases, but the n-π* transition requires less energy, hence the wavelength increases. Broad absorption peaks at long wavelengths can be attributed to intramolecular charge transfer (ICT) peaks from the DICz donor to the acceptor unit. The molecules in this case are solvent independent, which is described by the Frank-Condon Transition, which also explains the weak interaction between solvent and the molecule. The emission of **DICz-DBPZ** and **DICz-DPPN** in toluene at 559 nm and 516 nm at an excitation wavelength of 480 nm exhibits a remarkable bathochromic shift of 97 nm and 78 nm, which is compatible with its red-shifted ^{1}CT absorption band (**Fig. 2**). The shift demonstrated that the compounds are solvent polarity dependent, confirming the strong electron-accepting properties. This solvent-dependent nature can be explained by Photo-Induce Electron Transfer (PET).

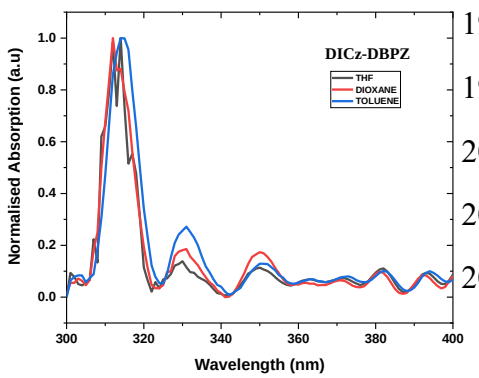

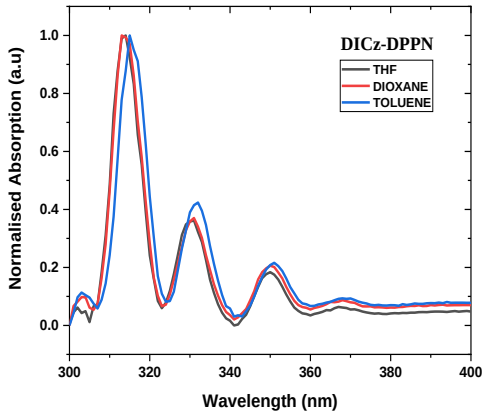

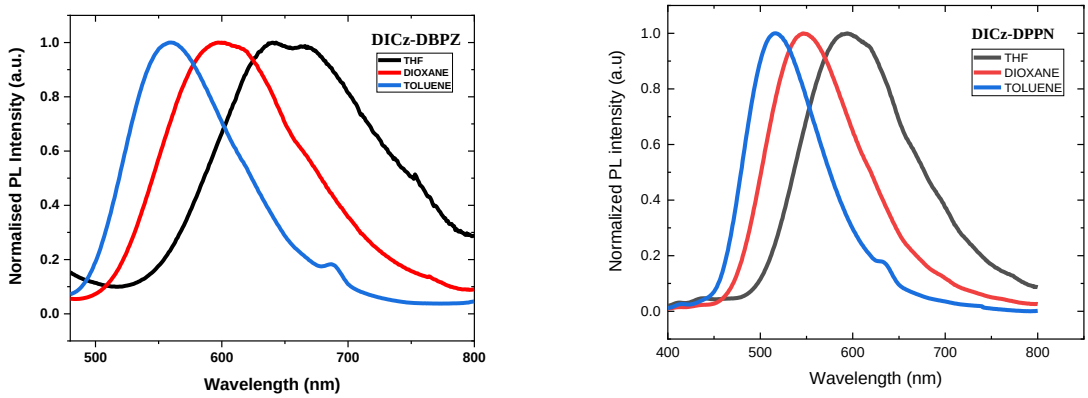

Fig 2: Ultraviolet-visible (UV-vis) and photoluminescence (PL) spectra of **DICz-DPPN** and **DICz-DBPZ** at room temperature.

Electrochemical properties:

To examine the HOMO-LUMO energy levels of two compounds, **DICz-DPPN** and **DICz-DBPZ**, a three-electrode cell system was used for Cyclic Voltammetry (CV). The cyclic voltammetry experiment was carried out with tetrabutylammonium hexafluorophosphate ($TBAPF_6$) in DCM (0.1 M) as a supporting electrolyte for the oxidation and tetrabutylammonium perchlorate (TBAP) in DMF for reduction potential. Both molecules showed an irreversible oxidation peak potential. Overall onset oxidation potentials were 1.04 and 0.94 for **DICz-DPPN** and **DICz-DBPZ** emitters, respectively (**Fig. 3**). The HOMO energy levels were calculated from the onset of the oxidation potential using the formula HOMO (eV) = - (E_{ox}onset – 0.44) - 4.80 eV and appear at -5.4eV and -5.3eV, whereas the LUMO energy levels were calculated from the onset of the reduction potential using the equation LUMO =

HOMO + Eg and appear at -1.66eV and -1.54eV and the resulting band gap energy was 3.74 eV and 3.76 eV for **DICz-DPPN** and **DICz-DBPN**, respectively.

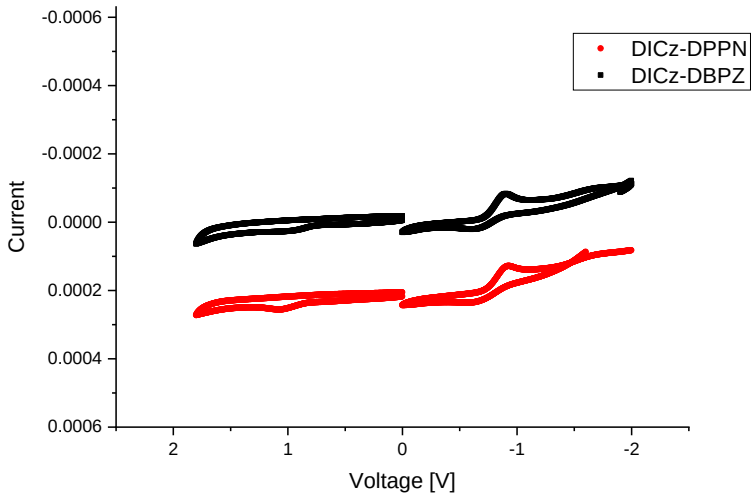

Fig. 3: Cyclic voltammograms of **DICz-DPPN** and **DICz-DBPN** in DCM with a scan rate of 100mVs^{-1}

Table.1 – Photophysical, thermal and electrical parameters of DICz-DPPN and DICz-DBPN TADF emitters

Compound	λ_{abs} (nm)	λ_{PL} (nm)	HOMO (ev)	LUMO (ev)	E_g(eV)	T_d (^{0}C)	T_g (^{0}C)
DICz-DPPN	314, 368	516	-5.4	-1.66	3.74	213	359
DICz-DBPZ	314, 393	559	-5.3	-1.54	3.76	269	378

Theoretical Studies:

Theoretical studies were carried out to understand the differences in optical properties of the synthesized molecules. The geometries of the two molecules were optimized by Density Functional Theory (DFT) using the popular B3LYP functional and 6-31G** basis set. The choice of the functional and the basis set were based on the constituting atoms in the molecules. Since both organic molecules are composed of carbon, hydrogen, nitrogen atoms in strongly conjugated aromatic rings; B3LYP level of theory was found suitable with a split valence basis

set 6-31G** having additional polarization function. The optimized geometries (**Table 2**) showed no negative frequencies indicating energy minima for the molecules.

Table 2: Optimized geometries of DICz_DBPZ and DICz_DPPN using B3LYP functional with 6-31G basis set**

Molecule	Optimized Structure
DICz_DBPZ	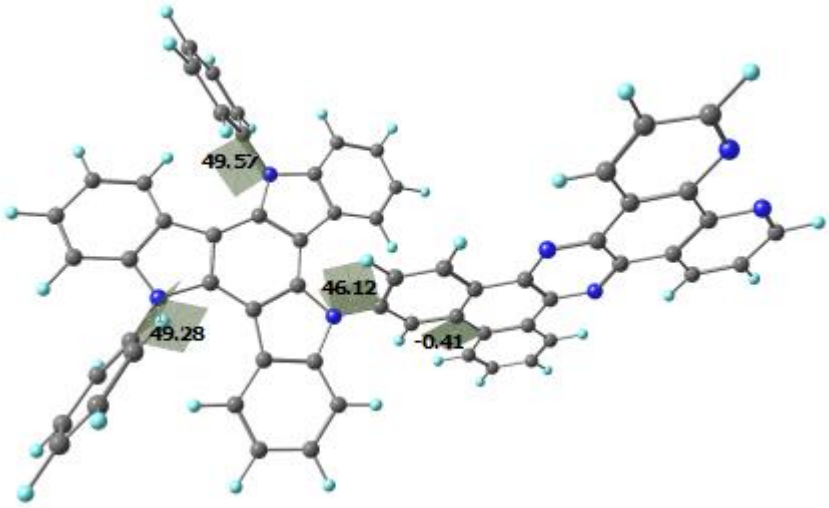
DICz_DPPN	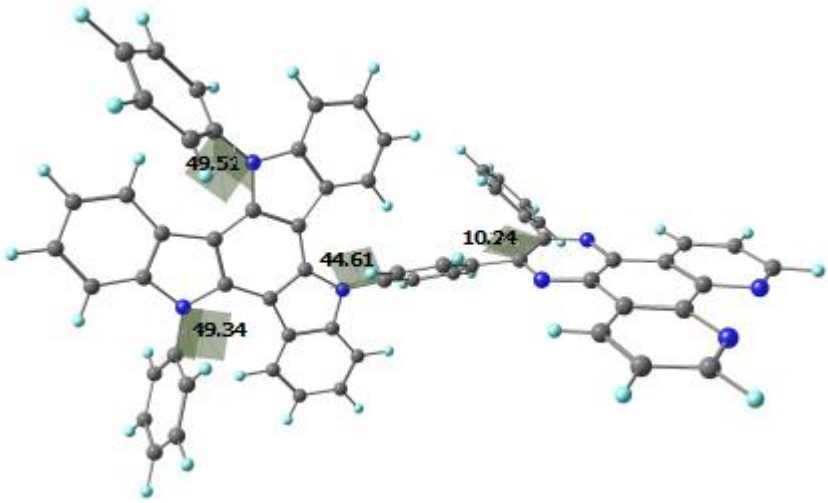

Population analysis was then done to visualize the molecular orbitals involved in the electronic transitions. The HOMO was found to reside predominantly on the donor moiety whereas the LUMO was largely populated on the acceptor in both the molecules. The table also shows orbital populations of other orbitals which are involved in the first five electronic transitions in TDDFT. (**Table 3**)

Table 3: Orbital plots of different molecular orbitals of DICz_DBPZ and DICz_DPPN from population analysis

Molecule	FMOs	
DICz_DBPZ	HOMO 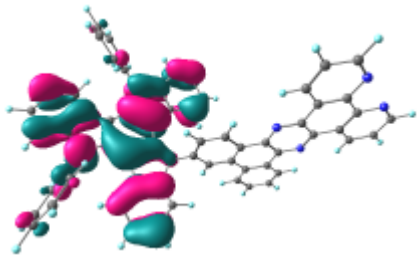	LUMO 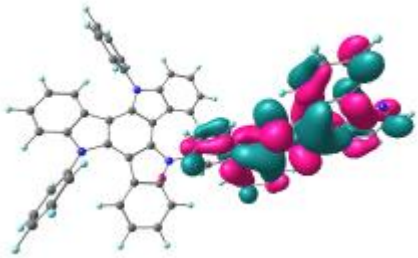
	HOMO-1 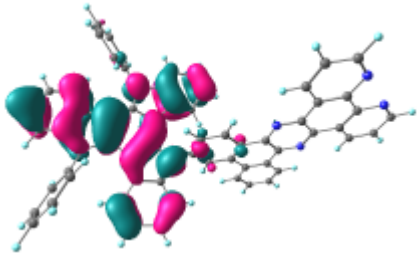	LUMO+1 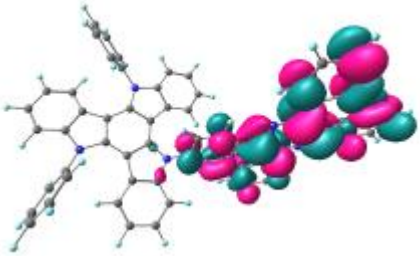
	HOMO-2 	LUMO+2 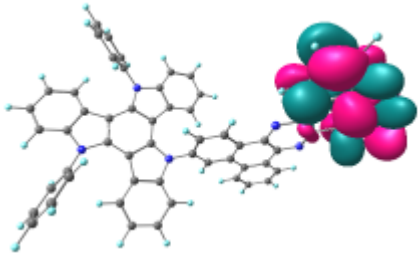
DICz_DPPN	HOMO 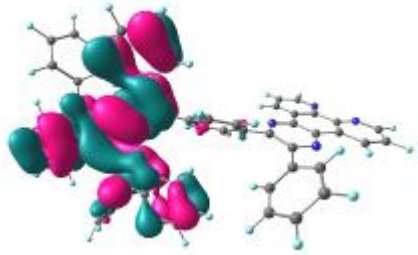	LUMO 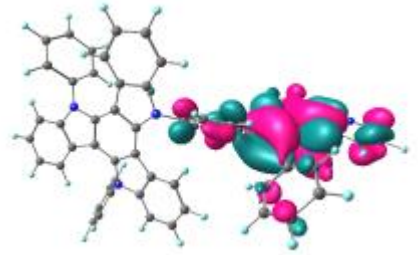
	HOMO-1	LUMO+1

	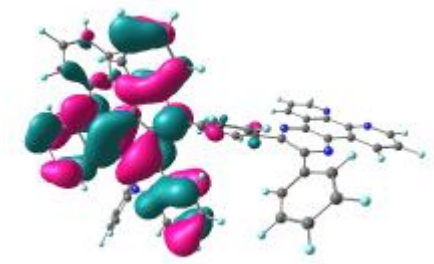	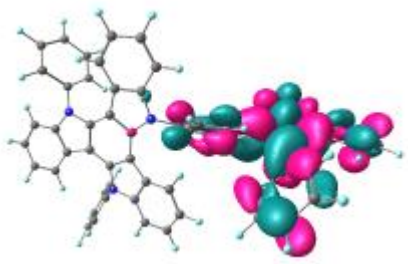
	HOMO-2 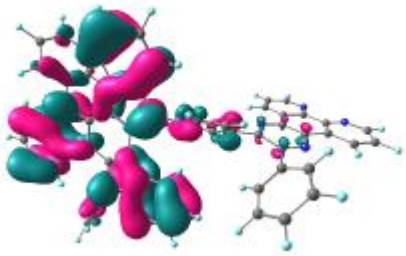	LUMO+2 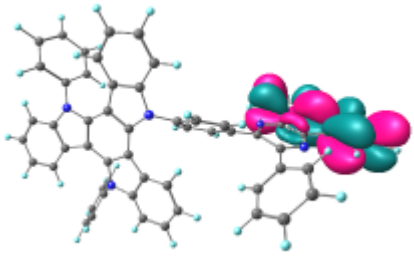

The optimized coordinates of the molecules were then used to predict the absorption spectrum of the two molecules. TD-DFT was performed using the same B3LYP functional with the 6-31G** basis set. Since the molecules exhibited long range conjugation, the computation was performed for 10 states (Nroots=10) to get a complete absorption profile of the molecule. Complete data of the first five states is tabulated in **Table 4**.

Table 4: Absorption maxima (λ_{max}), oscillator strength (*f*), major transitions (MT), weight in % (% C_i), Energy of transitions (eV) of the first five states

Molecule	States	Absorption (nm)	*f*	M.T.	%Ci
DICz_DBPZ	S1	551	0.029	H-1 → L	38
				H → L	61
	S2	548	0.026	H-1 → L	62
				H → L	38
	S3	439	0.041	H-1 → L+1	55
				H → L+1	42
	S4	437	0.022	H-1 → L+1	42

				H → L+1	56
	S5	415	0.095	H-2 → L	97
DICz_DPPN	S1	487	0.060	H-1 → L	82
				H → L	16
	S2	484	0.007	H-1 → L	16
				H → L	83
	S3	441	0.047	H-1 → L+1	81
				H → L+1	16
	S4	438	0.006	H-1 → L+1	16
				H → L+1	82
	S5	382	0.001	H-1 → L+2	64
				H → L+2	35

Device performance

OLEDs Fabrication and Performance

Regarding the favorable physical properties, these TADF compounds exhibiting intense emissions were employed as emitters in OLED fabrication to explore their potential for electroluminescent applications. Given the emission colors of these phenanthroline-based TADF emitters span from green to yellow, it is crucial to meticulously choose the appropriate host materials and the corresponding adjacent carrier transport layers to achieve efficient exothermic energy transfer. 1,1-bis[(di-4-tolylamino)phenyl]cyclohexane (TAPC) and 4,4',4"-tris(carbazol-9-yl)-triphenylamine (TCTA) were used to generate a step-wise hole transport, aiming to promote smooth hole injection from the hole transporting layer (HTL) into the emitting layer (EML).[27] Conversely, as the electron transporting layer (ETL) situated between the EML and the lithium fluoride (LiF)-electron injection layer (EIL), we selected a wide triplet-energy-bandgap material, bis-4,6-(3,5-di-3-pyridylphenyl)-2-methylpyrimidine (B3PyMPM).[28] Herein, we present the EML configuration in the proposed device architecture, utilizing an exciplex host to enhance current density and expand the carrier recombination zone.[29] This choice facilitates both exciton confinement and efficient electron transport. Moreover, we selected TCTA:B3PyMPM as the exciplex host to assist efficient

emission from the emitters due to its matched energy levels between the host and the guest.[30]Therefore, the carrier transport layers neighboring the EML were constructed using the same materials as the host, enhancing the current density and eliminating the energy barrier. Additionally, our device architecture incorporates a composite structure of HIL composed of a TAPC layer and a TAPC doped with MoO_3 layer, enabling a smooth hole injection from the ITO anode to the organic layer [5]. The thickness of each layer and the emitter concentrations were carefully regulated to maximize efficiency. For instance, in Fig. S1, various **DICz-DBPz**-based devices with different doping concentrations are depicted, revealing that the most favorable doping concentration is 5 wt %. As a result, the optimized architecture for the tested devices was set to ITO (120 nm)/TAPC:MoO_3 20 wt.% (5 nm)/TAPC (30 nm)/TCTA (5 nm)/ TCTA:B3PyMPM:emitter (47.5:47.5:5) (20 nm)/B3PyMPM (50 nm)/LiF (0.8 nm)/Al (120 nm), where the aluminum was used as the cathode. The dopant materials adopted in the devices are as follows: **DICz-DPPN** for device A; **DICz-DBPz** for device B. The corresponding chemical structures of the employed materials and the schematic structures of the fabricated TADF OLEDs are presented in Figs. 4(a) and 1(b).

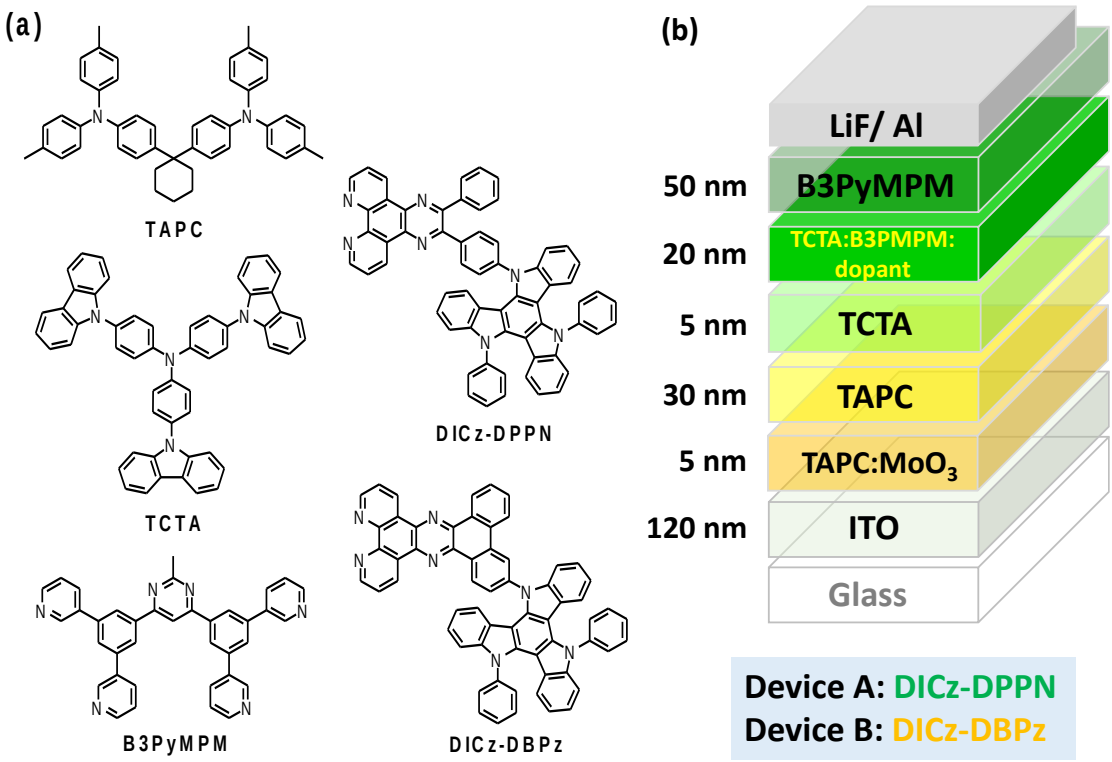

Figure 4. (a) Structural drawings of the materials used in OLEDs and (b) schematic structures of the fabricated OLEDs with different emitters.

Figure 5 and Table 5 summarize the EL characteristics and numerical data of the tested devices with different TADF emitters. Figure 5(a) illustrates that the emission spectral characteristics of all OLEDs align with the photoluminescence (PL) of the dopants. This alignment suggests that carrier recombination was confined within the EML, successfully preventing exciton diffusion to neighboring layers in both devices. [31] In addition, the green and yellow devices displayed spectral profiles devoid of distinctive features. The respective full width at half maximum (FWHM) are considered 120 and 109 nm. Consequently, the green and yellow devices maintained stable CIE coordinates of (0.37, 0.53) and (0.46, 0.52), respectively, across a luminance range of 1 to 1000 cd/m². The current density-voltage-luminance (*J-V-L*) characteristics of the tested devices are depicted in Fig. 5(b). As evident from the data, device B exhibited a slightly higher current density than device A. Since both devices have identical architectures, the increased current densities in device B can be attributed to the synergistic impact of reduced carrier trapping and enhanced carrier transport capabilities of **DICz-DBPz**. The respective turn-on voltages defined at a luminance value of 1 cd/m^2 of devices A and B are recorded at 2.5 and 2.3 V. In contrast, the luminance curves of device B showed much higher values than device A, indicating superior electroluminescence (EL) efficiency. Device A had a maximum luminance of 4541 cd/m^2 at an operating voltage of 10.6 V, while device B only achieved a much higher maximum luminance of 26142 cd/m^2 at the same voltage.

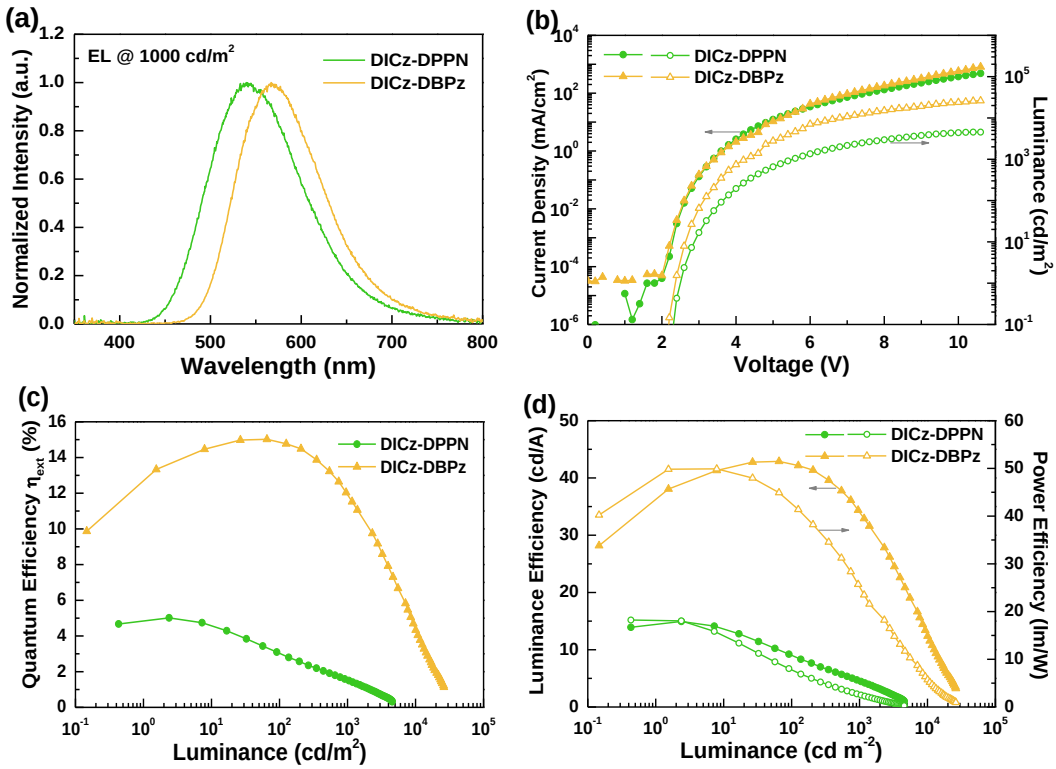

Figure 5. (a) Normalized EL spectra at a luminance of 100 cd/m^2; (b) current density−voltage−luminance (J−V−L) characteristics; (c) external quantum efficiency vs luminance; (d) luminance/power efficiency vs luminance for devices A (**DICz-DPPN**) and B (**DICz-DBPz**).

Table 5. EL characteristics of the devices with different TADF emitters.

Device		**A**	**B**
Host		**TCTA:B3PyMPM (1:1)**	**TCTA:B3PyMPM (1:1)**
TADF emitter (5 wt.%)		**DICz-DPPN**	**DICz-DBPz**
External quantum efficiency (%)	[a]	5.0	15.0
	[b]	3.0	14.9
Luminance efficiency (cd/A)	[a]	14.9	42.9
	[b]	9.1	42.5
Power efficiency (lm/W)	[a]	18.2	49.9
	[b]	7.8	42.9
V_{on} (V)	[c]	2.5	2.3
$\lambda_{max.}$ (nm)	[b]	539.5	567.0
FWHM (nm)	[b]	120	109
Max. Luminance (cd/m^2)		4541 [10.6]	26142 [10.6]
CIE1931 Coordinates (x, y)	[b]	(0.37, 0.53)	(0.47, 0.51)
	[d]	(0.37, 0.53)	(0.46, 0.52)

[a] Maximum efficiency; [b] measured at 10^2 cd/m^2; [c] turn-on voltage measured at 1 cd/m^2; [d] measured at 10^3 cd/m^2.

Conclusion:

Using DICz and phenanthroline as the donor-acceptor combination, two highly efficient and stable yellow-green TADF emitters, DICz-DBPZ and DICz-DPPN, were developed. In order to determine the relationship between theoretical and experimental results, the photophysical, thermal, electrochemical, and electroluminescent properties of the two emitters were extensively investigated. Utilizing DICz-DBPZ and DICz-DPPN emitters, respectively, the OLED device was able to emit the yellow emission peak at 567 nm with a colour coordinate of (0.47, 0.51) and the green emission peak at 539 nm with a colour coordinate of (0.37, 0.53). In comparison to the DICz-DPPN molecule, which displayed an EQE of 5% with a luminance efficiency of 14.9 lm/W, the DBPZ acceptor-based DICz-DBPZ was favorable in achieving a high EQE of 15% with a luminance efficiency of 42.9 lm/W.

References:

[1] C. W. Tang and S. A. Vanslyke, "Organic electroluminescent diodes," *Appl Phys Lett*, vol. 51, no. 12, pp. 913–915, 1987, doi: 10.1063/1.98799.

[2] K. Goushi, K. Yoshida, K. Sato, and C. Adachi, "Organic light-emitting diodes employing efficient reverse intersystem crossing for triplet-to-singlet state conversion," *Nat Photonics*, vol. 6, no. 4, pp. 253–258, Apr. 2012, doi: 10.1038/nphoton.2012.31.

[3] M. Y. Wong and E. Zysman-Colman, "Purely Organic Thermally Activated Delayed Fluorescence Materials for Organic Light-Emitting Diodes," *Advanced Materials*, vol. 29, no. 22. Wiley-VCH Verlag, Jun. 13, 2017. doi: 10.1002/adma.201605444.

[4] Z. Yang *et al.*, "Recent advances in organic thermally activated delayed fluorescence materials," *Chemical Society Reviews*, vol. 46, no. 3. Royal Society of Chemistry, pp. 915–1016, Feb. 07, 2017. doi: 10.1039/c6cs00368k.

[5] S. S. Kothavale and J. Y. Lee, "Three- and Four-Coordinate, Boron-Based, Thermally Activated Delayed Fluorescent Emitters," *Advanced Optical Materials*, vol. 8, no. 22. Wiley-VCH Verlag, Nov. 01, 2020. doi: 10.1002/adom.202000922.

[6] H. Uoyama, K. Goushi, K. Shizu, H. Nomura, and C. Adachi, "Highly efficient organic light-emitting diodes from delayed fluorescence," *Nature*, vol. 492, no. 7428, pp. 234–238, Dec. 2012, doi: 10.1038/nature11687.

[7] Y. Tao *et al.*, "Thermally activated delayed fluorescence materials towards the breakthrough of organoelectronics," *Advanced Materials*, vol. 26, no. 47. Wiley-VCH Verlag, pp. 7931–7958, Dec. 23, 2014. doi: 10.1002/adma.201402532.

[8] S. Kothavale, W. J. Chung, and J. Y. Lee, "Isomer engineering of dipyrido[3,2-a:3′,4′-c]phenazine-acceptor-based red thermally activated delayed fluorescent emitters," *J Mater Chem C Mater*, vol. 10, no. 15, pp. 6043–6049, Mar. 2022, doi: 10.1039/d2tc00017b.

[9] Y. J. Cho, S. K. Jeon, S. S. Lee, E. Yu, and J. Y. Lee, "Donor Interlocked Molecular Design for Fluorescence-like Narrow Emission in Deep Blue Thermally Activated Delayed Fluorescent Emitters," *Chemistry of Materials*, vol. 28, no. 15, pp. 5400–5405, Aug. 2016, doi: 10.1021/acs.chemmater.6b01484.

[10] G. Meng, X. Chen, X. Wang, N. Wang, T. Peng, and S. Wang, "Isomeric Bright Sky-Blue TADF Emitters Based on Bisacridine Decorated DBNA: Impact of Donor Locations on Luminescent and Electroluminescent Properties," *Adv Opt Mater*, vol. 7, no. 11, Jun. 2019, doi: 10.1002/adom.201900130.

[11] D. Y. Chen *et al.*, "Isomeric Thermally Activated Delayed Fluorescence Emitters for Color Purity-Improved Emission in Organic Light-Emitting Devices," *ACS Appl Mater Interfaces*, vol. 8, no. 26, pp. 16791–16798, Jul. 2016, doi: 10.1021/acsami.6b03954.

[12] Z. P. Chen *et al.*, "Optimization on Molecular Restriction for Highly Efficient Thermally Activated Delayed Fluorescence Emitters," *Adv Opt Mater*, vol. 6, no. 24, Dec. 2018, doi: 10.1002/adom.201800935.

[13] J. Jayakumar *et al.*, "Pyridine-Carbonitrile-Carbazole-Based Delayed Fluorescence Materials with Highly Congested Structures and Excellent OLED Performance," *ACS Appl Mater Interfaces*, vol. 11, no. 23, pp. 21042–21048, Jun. 2019, doi: 10.1021/acsami.9b04664.

[14] T. L. Wu, S. H. Lo, Y. C. Chang, M. J. Huang, and C. H. Cheng, "Steric Switching for Thermally Activated Delayed Fluorescence by Controlling the Dihedral Angles between Donor and Acceptor in Organoboron Emitters," *ACS Appl Mater Interfaces*, vol. 11, no. 11, pp. 10768–10776, Mar. 2019, doi: 10.1021/acsami.8b21568.

[15] S. Xiang *et al.*, "To improve the efficiency of thermally activated delayed fluorescence OLEDs by controlling the horizontal orientation through optimizing stereoscopic and linear structures of indolocarbazole isomers," *J Mater Chem C Mater*, vol. 6, no. 21, pp. 5812–5820, 2018, doi: 10.1039/c8tc01419a.

[16] S. Y. Byeon, J. Kim, D. R. Lee, S. H. Han, S. R. Forrest, and J. Y. Lee, "Nearly 100% Horizontal Dipole Orientation and Upconversion Efficiency in Blue Thermally Activated Delayed Fluorescent Emitters," *Adv Opt Mater*, vol. 6, no. 15, Aug. 2018, doi: 10.1002/adom.201701340.

[17] H. Nakanotani *et al.*, "High-efficiency organic light-emitting diodes with fluorescent emitters," *Nat Commun*, vol. 5, May 2014, doi: 10.1038/ncomms5016.

[18] Z. Ge *et al.*, "Novel bipolar bathophenanthroline containing hosts for highly efficient phosphorescent OLEDs," *Org Lett*, vol. 10, no. 3, pp. 421–424, Feb. 2008, doi: 10.1021/ol702773d.

[19] Y. Tao, C. Yang, and J. Qin, "Organic host materials for phosphorescent organic light-emitting diodes," *Chem Soc Rev*, vol. 40, no. 5, pp. 2943–2970, Apr. 2011, doi: 10.1039/c0cs00160k.

[20] B. Carlson *et al.*, "Divalent osmium complexes: Synthesis, characterization, strong red phosphorescence, and electrophosphorescence," *J Am Chem Soc*, vol. 124, no. 47, pp. 14162–14172, Nov. 2002, doi: 10.1021/ja0176705.

[21] N. D. McClenaghan *et al.*, "Ruthenium(II) dendrimers containing carbazole-based chromophores as branches," *J Am Chem Soc*, vol. 125, no. 18, pp. 5356–5365, May 2003, doi: 10.1021/ja021373y.

[22] H. Suzuki, T. Kanbara, and T. Yamamoto, "Ru(II) complexes with new redox-active 1,10-phenanthroline derivatives: Structural, spectral, and electrochemical investigations," *Inorganica Chim Acta*, vol. 357, no. 14, pp. 4335–4340, Nov. 2004, doi: 10.1016/j.ica.2004.06.027.

[23] W. Y. Wong, G. J. Zhou, X. M. Yu, H. S. Kwok, and Z. Lin, "Efficient organic light-emitting diodes based on sublimable charged iridium phosphorescent emitters," *Adv Funct Mater*, vol. 17, no. 2, pp. 315–323, Jan. 2007, doi: 10.1002/adfm.200600359.

[24] G. Zucchi *et al.*, "Solution, solid state, and film properties of a structurally characterized highly luminescent molecular europium plastic material excitable with visible light," *Inorg Chem*, vol. 50, no. 11, pp. 4851–4856, Jun. 2011, doi: 10.1021/ic2000415.

[25] D. H. Ahn *et al.*, "Highly efficient blue thermally activated delayed fluorescence emitters based on symmetrical and rigid oxygen-bridged boron acceptors," *Nat Photonics*, vol. 13, no. 8, pp. 540–546, Aug. 2019, doi: 10.1038/s41566-019-0415-5.

[26] J. H. Kim, K. H. Lee, and J. Y. Lee, "Design of thermally activated delayed fluorescent sensitizers for high efficiency over 20% and long lifetime in yellow fluorescent organic light-emitting diodes," *J Mater Chem C Mater*, vol. 8, no. 15, pp. 5265–5272, Apr. 2020, doi: 10.1039/d0tc00178c.

[27] T. C. Yiu *et al.*, "Multifaceted Sulfone-Carbazole-Based D-A-D Materials: A Blue Fluorescent Emitter as a Host for Phosphorescent OLEDs and Triplet-Triplet Annihilation Up-Conversion Electroluminescence," *ACS Appl Mater Interfaces*, 2022, doi: 10.1021/acsami.2c21294.

[28] R. H. Yi *et al.*, "Dicyano-Imidazole-Based Host Materials Possessing a Balanced Bipolar Nature to Realize Efficient OLEDs with Extremely High Luminance," *Journal of Physical Chemistry C*, vol. 124, no. 37, pp. 20410–20423, Sep. 2020, doi: 10.1021/acs.jpcc.0c05418.

[29] D. Luo *et al.*, "Approach to Fast Screen the Formation of an Exciplex," *Journal of Physical Chemistry C*, vol. 124, no. 18, pp. 10175–10184, May 2020, doi: 10.1021/acs.jpcc.0c00825.

[30] Y. S. Park, S. Lee, K. H. Kim, S. Y. Kim, J. H. Lee, and J. J. Kim, "Exciplex-forming Co-host for organic light-emitting diodes with ultimate efficiency," *Adv Funct Mater*, vol. 23, no. 39, pp. 4914–4920, Oct. 2013, doi: 10.1002/adfm.201300547.

[31] A. Jouaiti *et al.*, "True- to Sky-Blue Emitters Bearing the Thiazolo[5,4-d]thiazole Electron Acceptor for Single and Tandem Organic Light-Emitting Diodes," *ACS Appl Electron Mater*, May 2023, doi: 10.1021/acsaelm.3c00234.

[32] W. L. Chen *et al.*, "A method to realize efficient deep-red phosphorescent OLEDs with a broad spectral profile and low operating voltages," *Materials*, vol. 14, no. 19, Oct. 2021, doi: 10.3390/ma14195723.

Supporting Information

Yellow-emitting device B (DICz-DBPz) with different doping concentrations

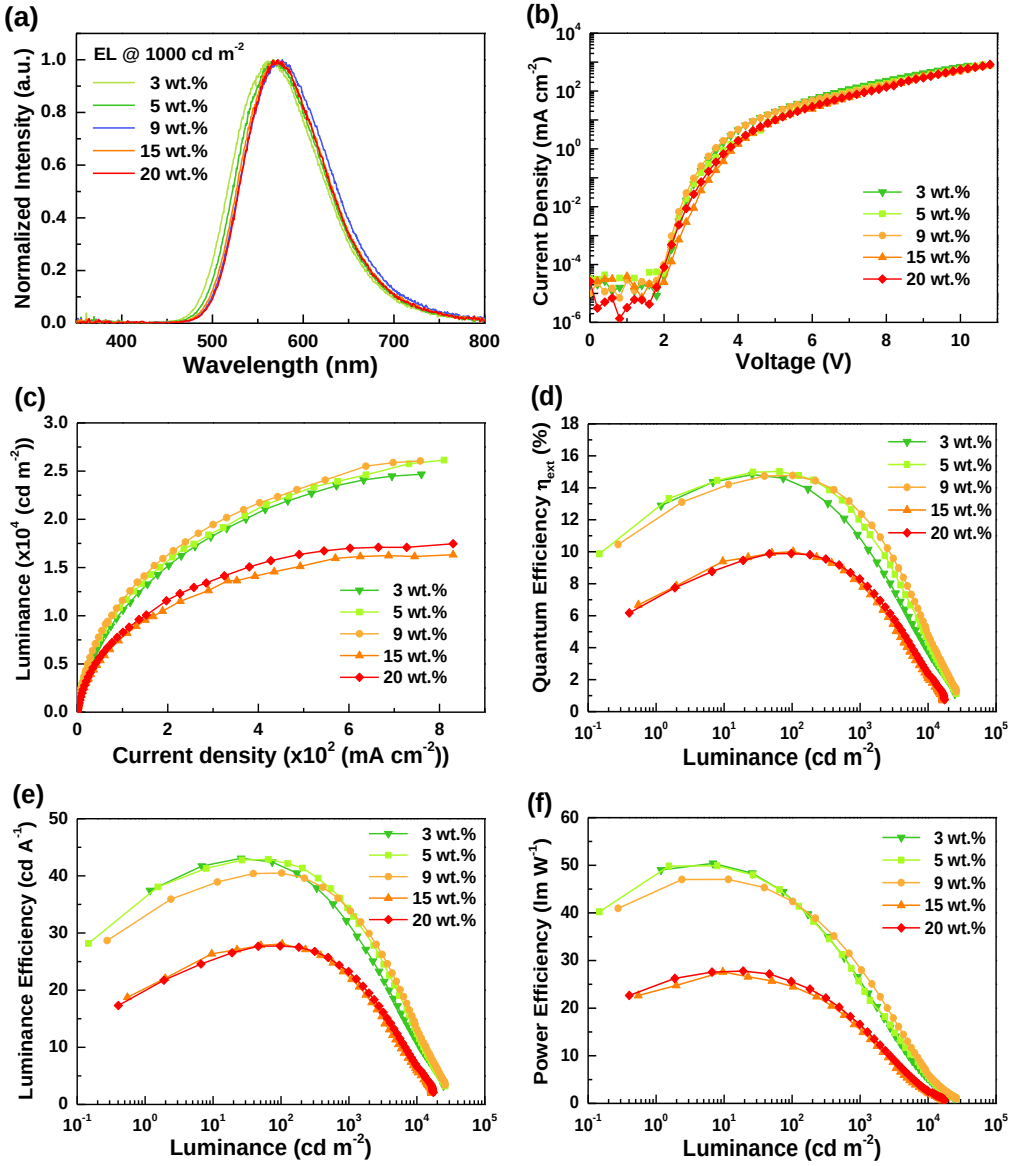

Fig. S1. (a) Normalized EL spectra at a luminance of 10^2 cd m^{-2}; (b) current density– voltage (*J*–*V*) characteristics; (c) luminance–current density (*L*–*J*) characteristics; (d) external quantum efficiency (EQE) vs. luminance; (e) luminance efficiency vs. luminance; (f) power efficiency vs. luminance for devices B (**DICz-DBPz**) with different doping concentrations.

Table S1. EL characteristics of the device B with different doping concentrations.

Host	**TCTA:B3PyMPM (1:1)**

Doping concentration of DICz-DBPz (%)		**3**	**5**	**9**	**15**	**20**
External quantum efficiency (%)	[a]	14.8	15.0	14.8	10.0	9.9
	[b]	14.4	14.9	14.8	10.0	9.8
Luminance efficiency (cd/A)	[a]	43.1	42.9	40.5	28.1	27.7
	[b]	41.9	42.5	40.5	28.1	27.7
Power efficiency (lm/W)	[a]	50.4	49.9	47.0	27.6	27.8
	[b]	43.1	42.9	42.5	24.6	25.5
V_{on} (V)	[c]	2.4	2.3	2.3	2.6	2.4
$\lambda_{max.}$ (nm)	[b]	567.0	567.0	577.0	567.0	572.0
FWHM (nm)	[b]	112	109	111	107	104
Max. Luminance (cd/m^2)		24674 [10.4]	26142 [10.6]	26058 [10.8]	16327 [10.8]	17467 [10.8]
CIE1931 Coordinates (x, y)	[b]	(0.46, 0.52)	(0.47, 0.51)	(0.49, 0.50)	(0.47, 0.51)	(0.48, 0.51)
	[d]	(0.44, 0.53)	(0.46, 0.52)	(0.48, 0.51)	(0.47, 0.51)	(0.48, 0.51)
	[e]	(0.44, 0.53)	(0.46, 0.52)	(0.47, 0.51)	(0.47, 0.51)	(0.47, 0.51)

[a] Maximum efficiency; [b] measured at 10^2 cd/m^2; [c] turn-on voltage measured at 1 cd m^{-2}; [d] measured at 10^3 cd/m^2; [e] measured at 10^4 cd/m^2.